GPM6B inhibits tumor progression by targeting HPGD in lung adenocarcinoma

YONGHUAI LI[1,2*], XUFENG YAO[3*], QIAN CHAI[1,2], XUEYI FENG[3], YUHAO MA[3], GUOMENG LI[3], HONGBIN ZHU[4], LEI ZHAO[1,2,5] and QIAN DAI[3,6,7]

[1]Department of Respiratory Medicine, The First Affiliated Hospital of Anhui Medical University, Hefei, Anhui 230012, P.R. China; [2]Department of Respiratory Medicine, Anhui Public Health Clinical Center, Hefei, Anhui 230012, P.R. China; [3]School of Life Science, Anhui Medical University, Hefei, Anhui 230032, P.R. China; [4]Department of Respiratory Medicine, Chaohu Hospital of Anhui Medical University, Chaohu, Anhui 238000, P.R. China; [5]Department of Respiratory Medicine, Fuyang Affiliated Hospital of Anhui Medical University, Fuyang, Anhui 236000, P.R. China; [6]Department of Respiratory Medicine, The First Affiliated Hospital of Anhui Medical University, Hefei, Anhui 230012, P.R. China; [7]Department of Respiratory Medicine, Anhui Public Health Clinical Center, Hefei, Anhui 230012, P.R. China

Received October 5, 2024; Accepted March 20, 2025

DOI: 10.3892/mmr.2025.13618

Abstract. Lung adenocarcinoma (LUAD) is the most prevalent form of lung cancer and the predominant cause of cancer-associated mortality. Given the low survival rate of patients with LUAD, there is a need to identify new therapeutic targets. Glycoprotein M6B (GPM6B) is a tumor-associated gene in numerous types of malignancies; however, its specific role in LUAD remains largely unexplored. Integrated bioinformatics analyses of The Cancer Genome Atlas and Gene Expression Omnibus datasets, along with immunohistochemistry assays demonstrated that GPM6B was downregulated in LUAD compared with adjacent normal tissue. Elevated expression of GPM6B was associated with prolonged survival in patients with LUAD, suggesting that GPM6B serves as a prognostic biomarker in LUAD. Cell Counting Kit-8 (CCK-8) and Transwell assays demonstrated that exogenously expressed GPM6B significantly inhibited the proliferation and migration of the LUAD cell lines A549 and PC9. Notably, tumorigenesis assays conducted in nude mice demonstrated that the overexpression of GPM6B also suppressed tumor growth *in vivo*. Mechanistically, GPM6B may have inhibited the malignant behavior of LUAD cells by promoting the expression of 15-hydroxyprostaglandin dehydrogenase and activating the p53 signaling pathway, as evidenced by transcriptome data analysis, western blotting and phenotypic assays. Furthermore, the qPCR results from LUAD cells treated with DNA methylation and histone deacetylase inhibitors indicated that low expression of GPM6B was associated with DNA methylation and histone deacetylation. Overall, the present study demonstrated that GPM6B may serve as a novel tumor suppressor and elucidated its potential mechanism in regulating the progression of LUAD.

Correspondence to: Dr Qian Dai, School of Life Science, Anhui Medical University, 81 Meishan Road, Shushan, Hefei, Anhui 230032, P.R. China
E-mail: daiqian@ahmu.edu.cn

Dr Lei Zhao, Department of Respiratory Medicine, The First Affiliated Hospital of Anhui Medical University, 100 Huaihai Avenue, Yaohai, Hefei, Anhui 230012, P.R. China
E-mail: ayefyzhaolei@163.com

*Contributed equally

Key words: lung adenocarcinoma, GPM6B, HPGD, p53 signaling pathway, DNA methylation, histone deacetylation

Introduction

Lung cancer has a notably high incidence and mortality rate, with an estimated 124,730 deaths in the United States in 2025 (1,2). Among types of lung cancer, lung adenocarcinoma (LUAD) is the most prevalent subtype (3). Several small molecule inhibitors of driver genes, including epidermal growth factor receptor, anaplastic lymphoma kinase and ROS proto-oncogene 1, have been designed as effective drugs (4-7). Furthermore, the combination of programmed cell death protein 1 (PD-1)/programmed cell death protein ligand 1 inhibitors with chemotherapy represents a treatment approach for both patients without driver gene mutations and those who have resistance to existing drugs (8,9). However, the 5-year survival rate of patients with lung cancer remains low, with a survival rate of 10% for small and 6-7% for non-small cell lung cancer, (10,11), due to the development of drug resistance and distant metastasis (12). Consequently, novel treatment targets for LUAD and its pathogenesis warrant further clinical research.

The epigenetic landscape, which includes DNA methylation, chromatin organization, histone modifications and non-coding RNA regulation, contributes to the expression of pro-oncogenes and tumor suppressor genes; the association between epigenetics and heterogeneous tumor microenvironments

makes the treatment of lung cancer a challenge (13,14). Loss of expression or low expression of tumor suppressor genes such as tumor protein p53, *PTEN* and *BRCA1* results in the occurrence and development of tumors and these genes are regarded as valuable targets in cancer treatment (15). DNA methylation, histone deacetylation and H3K27 methylation are key mechanisms that inhibit gene expression by recruiting suppressive proteins to the modified domains (16-18). Widespread aberrant patterns of DNA methylation, which is catalyzed DNA methyltransferases (DNMTs) such as DNMT3a, DNMT3b and DNMT1, are observed in lung cancer (19). Altered regulation of DNMTs has been detected in non-small cell lung cancer cells and is involved in the regulation of tumor growth (20,21). Histone deacetylases (HDACs) are enzymes that catalyze the deacetylation of histones, and they are commonly upregulated in lung cancer (17). The enhancer of zeste homolog 2 (EZH2) subunit of the polycomb repressive complex 2 is responsible for inducing H3K27 methylation (22). Targeting EZH2 has potential for the treatment of lung cancer, as it has been reported that EZH2 inhibition can overcome resistance to immunotherapy through blockade of PD-1 (23,24). The development of novel therapeutic approaches may be facilitated by understanding how epigenetic modifications in lung cancer progression cause mis-regulation of tumor suppressor genes. Glycoprotein M6B (GPM6B), a four transmembrane protein belonging to the proteolipid protein (PLP) family, exhibits a high degree of sequence similarity to PLP1 and GPM6A. GPM6B is primarily expressed in neurons, oligodendrocytes and activated astrocytes in the central nervous system. The primary functions of GPM6B are to mediate intercellular contact and regulate membrane growth, composition and targeting (25-27). Zhu *et al* (28) reported that microRNA-1908-3p promotes tumor proliferation and migration in breast cancer by targeting GPM6B. GPM6B inhibits the growth of prostate cancer by regulating the uptake of serotonin (29). Patients with glioma with high expression of GPM6B tend to exhibit prolonged survival (30). Furthermore, targeting GPM6B impairs the self-renewal and tumorigenicity of mesenchymal glioblastoma stem cells by inhibiting the activation of the Wnt pathway (30). The aforementioned studies demonstrate that GPM6B is implicated in the progression of solid malignant tumors. However, its specific function and underlying mechanisms within LUAD remain elusive.

The present study aimed to investigate the role of GPM6B in cell proliferation and migration in LUAD.

Materials and methods

Survival and expression analysis. Kaplan-Meier plotter (kmplot.com), which compiles publicly available datasets for analysis, was used to examine the effect of GPM6B and HPGD expression on the overall survival (OS) of patients with LUAD. The survival analysis included multiple regression analyses considering pathological type, age, gender, and smoking history, with the median expression level serving as the cutoff value. The Gene Expression Profiling Interactive Analysis (GEPIA; gepia.cancer-pku.cn/) and Gene Expression Omnibus (GEO; ncbi.nlm.nih.gov/geo/) (31) databases were used to determine the relative expression of GPM6B and HPGD in LUAD and normal tissues. The online software UALCAN (ualcan.path.uab.edu/analysis.html) was used to analyze the differential expression of GPM6B with respect to tumor, node, metastasis stage and nodal metastasis status, as well as to assess the levels of DNA methylation in the promoter region of GPM6B.

Nomogram construction. Spliced Transcripts Alignment to a Reference (STAR)-count data and clinical information relevant to LUAD were obtained from The Cancer Genome Atlas (TCGA) database (portal.gdc.cancer.gov) (32). LUAD dataset (portal.gdc.cancer.gov/projects/TCGA-LUAD) was used for analysis. The data were converted into transcript per million (TPM) format, and log2 (TPM + 1) normalization was performed.

R package 'rms' was used to construct a nomogram featuring clinical node stage, sex, age, tumor stage and the expression of GPM6B or HPGD. The analysis was performed using R version 4.0.0 (R Core Team, 2020). Through Cox regression analysis, a nomogram model was developed to evaluate the prognostic significance of these features across 476 samples and predict the survival rates of patients at 1, 3 and 5 years. LUAD samples was acquired from TCGA-LUAD dataset (portal.gdc.cancer.gov/projects/TCGA-LUAD) through the GDC Data Portal (portal.gdc.cancer.gov).

Clinical sample collection. LUAD and adjacent normal tissues were collected from the Pathology Department of Chaohu Hospital, Chaohu, China. The adjacent normal tissues were 1 cm from the margin of the LUAD tissue. Samples were obtained during the preliminary diagnosis of patients between January 2023 and January 2025, all of whom were diagnosed with LUAD based on pathological examination. Verbal informed consent was obtained from all participants. The study included six patients (four males and 2 female; age, 54-77 years) with a pathological diagnosis of lung adenocarcinoma were enrolled in the study. All procedures were approved by the Ethics Committee of Chaohu Hospital of Anhui Medical University (approval no. KYXM-202410-010). Tissue samples were used for immunohistochemistry (IHC) analysis.

Cell culture. Human LUAD A549 and PC9 and 293T cells were obtained from Procell Life Science and Technology Co., Ltd. All cells were cultured in DMEM (Biosharp Life Sciences) supplemented with 10% (v/v) fetal bovine serum (FBS; Shanghai ExCell Biology, Inc.) and 100 U/ml penicillin0streptomycin (Biosharp Life Sciences) at 37˚C with 5% carbon dioxide.

Plasmids and stable cell lines. GPM6B and HPGD coding sequences were downloaded from National Center for Biotechnology Information (NCBI; ncbi.nlm.nih.gov) and cloned into the pLJM1-EGFP vector (cat. no. 19319; Addgene, Inc.) via *Age*I and *Eco*RI enzyme sites. Coding sequences of GPM6B coupled with HA tag sequences were cloned into pLVX vector (cat. no. 632164; Clontech) via *BamH1* and *Eco*RI enzyme sites. The lentivirus were packaged with 2nd generation system. Briefly, the transfection of vectors into 293T cells was conducted at room temperature with a mixture consisting of 5.0 overexpression construct, 5.0 p8.9 packaging

plasmid and 2.5 μg VSVG envelope plasmid utilizing the Hieff Trans™ Liposomal Transfection Reagent (Shanghai Yeasen Biotechnology Co., Ltd.). The lentiviral particles were collected following 48 h transfection. A549 or PC9 cells were infected with in a 6-well plate with a multiplicity of infection of 0.5. After 10 h of infection, antibiotic selection with 2 μg/ml puromycin dihydrochloride (Biosharp Life Sciences) was used to generate the stable cell lines. Following selection for 72 h, the exogenous GPM6B-overexpressing stable A549 and PC9 cells were used for subsequent experiments. The negative control for GPM6B-overexpressing stable A549 cells was the A549 cell line transfected with the pLJM1 backbone plasmid. Similarly, the negative control for GPM6B-overexpressing stable PC9 cells was the PC9 cell line transfected with the pLJM1 backbone plasmid. Stably transfected A549 and PC9 cells were maintained with 1 μg/ml puromycin.

Reverse transcription-quantitative PCR (RT-qPCR). Total RNA was extracted from 1x10^6 A549 or PC9 cells using the SPARKeasy Tissue/Cell RNA kit (Shandong Sparkjade Scientific Instruments Co., Ltd.) and cDNA was synthesized using the MonScript™ RTIII All-in-One Mix with dsDNase (Monad Biotech Co., Ltd.), according to the manufacturer's instructions. qPCR was performed using the ChamQ Universal SYBR qPCR Master Mix (Vazyme Biotech Co., Ltd.). Thermocycling conditions were as follows: Initial denaturation for 30 sec at 95˚C for initial denaturation, followed by 40 cycles of 10 sec at 95˚C and 30 sec at 60˚C. Fold-changes in mRNA levels were determined using the comparative $2^{-\Delta\Delta Cq}$ method (33), with GAPDH or β-actin as the internal reference gene. The primer sequences used were as follows: GAPDH: forward, 5'-CAACTGCTTAGCACCCCTGG-3' and reverse, 5'-GTCAAAGGTGGAGGAGTGGG-3'; β-actin: forward, 5'-CATGTACGTTGCTATCCAGGC-3' and reverse, 5'-CTCCTTAATGTCACGCACGAT-3'; creatine kinase, mitochondrial 1A (CKMT1A): Forward, 5'-TCTCCTCCAGCACAGGAACT-3' and reverse, 5'-AAATGGGGGTCGGATTGGAG-3'; DSTN pseudogene 2 (DSTNP2): Forward, 5'-CATCAGATGCCTTTGAGACATACA-3' and reverse, 5'-TCTGGTGTGGAGCATTTACGAAC-3'; TNFSF12-TNFSF13 readthrough (TNFSF12-TNFSF13): Forward, 5'-GAAGCCAGAATCAACAGCTCC-3' and reverse, 5'-GCATCGGAACTCTGACAGTACAG-3'; eukaryotic translation initiation factor 4E binding protein 3 (EIF4EBP3): Forward, 5'-TGTCAACGTCCACTAGCTGC-3' and reverse, 5'-CTCCAGCAGGAACTTTCGGT-3'; Polyamine modulated factor 1 binding protein 1 (PMFBP1): forward, 5'-CACGCCTTTGACAAGAAGCTA-3' and reverse, 5'-TTGAGGTCATTCTGGTGTTGC-3'; Protocadherin alpha 12 (PCDHA12): forward, 5'-AGAGAGCAAACGCCAAAACTC-3' and reverse, 5'-CACATCCAGGACGGTTATTTGA-3'; Oxidized low density lipoprotein receptor 1 (OLR1): 5'-ACTCTCCATGGTGGTGCCTGG-3' and reverse, 5'-GCTTGTTGCCGGGCTGAGATCT-3'; Ankyrin repeat domain 1 (ANKRD1): Forward, 5'-AGCGCCCGAGATAAGTTGCT-3' and reverse, 5'-CACCAGATCCATCGGCGTCT-3'; Inhibin subunit βA (INHBA): Forward, 5'-CAACAGGACCAGGACCAAAGT-3' and reverse, 5'-GAGAGCAACAGTTCACTCCTC-3'; GPM6B: Forward, 5'-CGTGGCGATTCTTGAGCAAC-3' and reverse, 5'-CAGGCCACTCCAAGCACATA-3'; HPGD: Forward, 5'-AGCAGCCGGTTTATTGTGCTT-3' and reverse, 5'-GCGTGTGAATCCAACTATGCC-3' and EZH2: Forward, 5'-GGACCACAGTGTTACCAGCAT-3' and reverse, 5'-GTGGGGTCTTTATCCGCTCAG-3'.

Western blot. Protein extracts from 1x10^6 A549 or PC9 cells were prepared on ice using RIPA (cat. no. PR20035; Proteintech Group, Inc.) lysis buffer containing proteinase inhibitor. The total protein concentration was determined using a BCA Protein Quantification kit (Vazyme Biotech Co., Ltd.). Proteins were separated using 8% SDS-PAGE with 2 mg protein/well and transferred onto PVDF membranes. After 1 h blocking in 5% skimmed milk at room temperature, the PVDF membranes were incubated with primary antibodies against GAPDH (cat. no. GB15002; Servicebio; 1:10,000), GPM6B (cat. no. AB03180; Qizhidao Technology Co., Ltd.; 1:1,000 dilution), HPGD (cat. no. 66798-1-Ig; Wuhan Sanying Biotechnology, 1:5,000 dilution), P53 (cat. no. HY-P80257; MedChemExpress; 1:1,000 dilution), Cyclin D1 (CCND1; cat.no.380999), Bcl2 (cat.no.R23309; Chengdu Zen-Bioscience Co., Ltd.; 1:1,000 dilution) and Bax (cat. no. 200958; all Chengdu Zhengneng Biotechnology Co., Ltd.; all 1:1,000) overnight at 4˚C. The membranes were incubated the following horseradish peroxidase (HRP)-conjugated secondary antibodies: goat anti-rabbit IgG-HRP (cat. no. BL003A, White Shark Biotechnology Co., Ltd.; 1:10,000) and goat anti-mouse IgG-HRP (cat. no. BL001A, White Shark Biotechnology Co., Ltd.; 1:10,000 dilution) at room temperature for 2 h. The protein signals were detected using the SuperKine™ West Femto Maximum Sensitivity Substrate (Abbkine Scientific Co., Ltd.) and images were acquired using a multi-function imaging system (Vilber Lourmat).

Cell proliferation assay. Cell proliferation was evaluated using the Cell Counting Kit-8 (CCK-8) assay (Biosharp Life Sciences). Briefly, 2x10^3 cells were seeded into 15 wells of a 96-well plate. A total of 100 μl medium containing 10 μl CCK-8 regent was added at 1-5 days after seeding and the optical density at 450 nm was measured after 2 h.

Ki67 staining and flow cytometry analysis. Ki67 (cat. no. 350504; BioLegend, Inc.) is a commonly utilized marker for assessing the tumor proliferation index (34-36). was. Following 72 h infection, the A549 and PC9 cells were harvested and subjected to two washes with PBS, fixed for 3 h at 4˚C using cold 70% ethanol (Chinasun Specialty Products Co., Ltd.) and washed twice more with PBS. The cells were stained with PE anti-mouse/human Ki-67 (cat. no. 350504; BioLegend, Inc.; 1:20) at room temperature for 15 min. Flow cytometry analysis was performed using the phycoerythrin detection channel on a Beckman cytometer (Beckman Coulter, Inc.) to quantify the Ki67 signals. The results were analyzed using CytoExpert 2.4 software (Beckman Coulter, Inc.).

Cell migration and invasion assay. For the wound healing assay, 5x10^5 A549 or PC9 cells were seeded in a six-well plate. A scratch was made on the surface of the cell layer when the cell confluence reached 100%. The cells were maintained in DMEM containing 1% FBS after scratching. The cells were imaged every 24 h under a light microscope (ECLIPSE Ts2,

Nikon), and the migration distance was calculated. For the Transwell migration assay, $5x10^4$ A549 or PC9 cells were seeded in the upper chambers (8 μm) and maintained in serum-free DMEM, whereas DMEM supplemented with 10% FBS and 100 U/ml penicillin/streptomycin was added to the lower chambers. For the Transwell invasion assay, the bottom surface of each upper chamber was coated with Matrigel (BD Biosciences) for 1 h at 37˚C. A total of $5x10^4$ cells was seeded in the upper chambers. The cells were cultured at 37˚C for 14-16 h and fixed with 100% methanol at 4˚C for 20 min, stained the cells with 0.1% crystal violet at room temperature for 20 min and the imaged with inverted light microscope (ECLIPSE Ts2, Nikon).

Co-immunoprecipitation. A total of 10 ml of lentivirus packaged from the pLVX overexpression construct, along with 5.0 μg of the p8.9 packaging plasmid and 2.5 μg of VSVG, were used to infect $3x10^6$ 293T cells seeded in a 10-cm dish. After 72 h of infection, $1x10^7$ cells were harvested and lysed with 1 ml lysis buffer (cat. no. HY-K1000; MedChemExpress) at 4˚C with rotation for 4 h. The cell lysate was then centrifuged at 15,000 g for 15 min at 4˚C to collect the supernatant. A total of 1 μg of the primary antibody against IgG (cat. no. B900620; Proteintech) or HA (cat. no. 66006-2-Ig; Proteintech) as well as 50 μl Protein A/G agarose beads to the cell supernatant for incubation at 4˚C overnight. Following incubation, the Protein A/G agarose beads (cat. no. PR40025; Proteintech) were washed three times with PBS at 4˚C. The supernatant was then discarded, and 50 μl of 2xSDS (cat. no. P0015B; Beyotime) was added to the agarose beads. After vortexing at 500 x g for 10 sec at room temperature, the mixture was placed in a metal bath at 95˚C for 10 min. Finally, 10 μl of each sample was taken for Western blot experiments.

Nude mouse tumor xenograft model. Numerous studies have used the A549 cell line to establish tumor-bearing models (37-39). A total of 12 BALB-c nude mice were divided into a control group and a GPM6B-overexpressing group, each group containing six 5-week-old female mice (Biomart). All mice exhibited comparable body weights (~15 g). Mice were housed at 20-26˚C and the relative humidity is kept at 50-60%, 12/12-h light/dark cycle and *ad libitum* food and water. Mice were subcutaneously injected with ~$2x10^6$ cells into the right forelimb 1 week after purchase. During the experiment, the mice were observed daily to detect any signs of illness or adverse reactions. Tumor volume was measured every 3 days. At 33 days post-injection, the mice exhibited signs of anxiety, along with a noticeable decrease in appetite. Therefore, euthanasia was performed by cervical dislocation following anesthesia by inhalation of 2% isoflurane (cat. no. R510-22-10, RWD Life Science Co., Ltd.) in oxygen until the loss of eyelid reflexes and the onset of muscle relaxation were observed. Death was confirmed by cessation of pulse and breathing. Tumors were dissected and weighed. All animal care and experimental procedures adhered to ARRIVE guidelines and were approved by the Ethics Committee of Animal Experiments of Anhui Medical University (approval no. LLSC20242301).

IHC and hematoxylin and eosin (H&E) staining. Paraffin-embedded clinical samples and tumor tissue from mice were sliced into 5-μm thick sections and rehydrated using descending alcohol concentrations. Antigen retrieval was performed using a sodium citrate retrieval solution with a pH of 6.0 at 100˚C then allowed to cool. This heating and cooling cycle was repeated twice. Slides were washed three times with PBS at room temperature. Sections were sealed with 5% bovine serum albumin (Wuhan Servicebio Technology Co., Ltd.) at room temperature for 45 min. The clinical samples were incubated with antibodies against GPM6B (cat. no. PC11847S; Abmart Pharmaceutical Technology Co., Ltd.; 1:400) and HPGD (cat. no. 66798-1-Ig; Proteintech Group, Inc.; 1:400), while the mouse tissue samples were incubated with Ki67 primary antibody (cat. no. A11390; ABclonal Biotech Co., Ltd.; 1:500) overnight at 4˚C. The sections were washed three times with PBS for 5 min each and incubated with goat anti-rabbit IgG-HRP (cat. no. BL003A; Hefei White Shark Biotechnology Co., Ltd.; 1:300) or Goat anti-mouse IgG-HRP (cat. no. BL001A; Hefei White Shark Biotechnology Co., Ltd.; 1:300) at 25˚C for 50 min. The samples were washed with PBS, stained with diaminobenzidine and counterstained with hematoxylin (Wuhan Servicebio Technology Co., Ltd.) at room temperature for 3 min. Finally, ascending ethanol dehydration and resin sealing were performed. For H&E staining, paraffin-embedded mouse tissue sections were stained with hematoxylin at room temperature for 5 min. This was followed by eosin at room temperature for 15 sec. Finally, sections were visualized using a light microscope (ECLIPSE Ts2, Nikon).

Small interfering (si)RNA transfection and drug treatment. Human EZH2 siRNA was produced by Beijing Tsingke Biotech Co., Ltd. and transfected into LUAD cells. In brief, 20 μM siRNA was transfected into $3x10^5$ A549 or PC9 cells at room temperature using Lipofectamine 2000 (cat. no. CN2541156; Invitrogen; Thermo Fisher Scientific, Inc.). After 8 h of transfection, the medium was replaced with fresh complete DMEM and the cells were cultured at 37˚C for an additional 48 h before proceeding with subsequent experiments. The siRNA sequences were as follows: Negative control, 5'-UUCUCCGAACGU GUCACGU-3'; siEZH2#1, 5'-GAGGGAAAGUGUAUGAUA ATT-3' and siEZH2#2, 5'-GAGGUUCAGACGAGCUGAU-3'. Decitabine (DCA; cat. no. HY-A0004) and trichostatin A (TSA; cat. no. HY-15144; both MedChemExpress) stocks were prepared in dimethyl sulfoxide. LUAD cells were treated with 1, 3 and 5 TSA for 24 h, and 100, 500 and 1,000 μM DCA at 37˚C for 48 h.

Transcriptome sequencing. Total RNA from control and GPM6B overexpressing PC9 cells was extracted using the SPARKeasy Tissue/Cell RNA kit (cat. no. AC0205-B; Shandong Sparkjade Scientific Instruments Co., Ltd.). Library construction and RNA-sequencing (RNA-Seq) were performed by Shanghai Meiji Biopharmaceutical Technology Co., Ltd. with Illumina NovaSeq 6000 (Illumina Inc.). The sequencing library was prepared using the Stranded Total RNA Prep with Ribo-Zero Plus kit (cat. no. 20040529; Illumina, Inc.). RNA samples meeting the following criteria were selected for library preparation: ≥1 μg total RNA at a concentration of ≥30 ng/μl, with an RNA Quality Number >6.5 (Agilent 5300) and A260/A280 ratios of 1.8-2.2 (Nanodrop 2000). RNA integrity was verified by agarose gel electrophoresis. Libraries were prepared using the Illumina® Stranded mRNA

Prep Kit (Illumina) and quantified via Qubit fluorometry (cat. no. Q33327; Thermo Fisher), adjusting the final working concentration to 3 ng/μl. Finally, paired-end sequencing with a read length of 150 bp was performed.

Differential expression analysis. After acquiring gene read counts, a differential expression analysis was conducted across multiple samples (≥2) to identify differentially expressed genes (DEGs) between sample groups, thereby facilitating subsequent functional studies of these DEGs. The analysis was carried out using DESeq2 (version: 1.44.0: http://bioconductor.org/packages/stats/bioc/DESeq2/). The criteria for significant differential expression were set as follows: P<0.05 and |log2FC|≥1.

Gene ontology (GO) analysis. GO enrichment analysis was conducted using GOATools software (https://github.com/tanghaibao/GOatools), employing the Fisher's exact test as the statistical method. To control for false positives, four multiple testing correction methods-Bonferroni, Holm, Sidak and false discovery rate-were applied to adjust the p-values. Generally, a Gene Ontology (GO) term is deemed significantly enriched when the adjusted P-value is less than 0.05.

Kyoto Encyclopedia of Genes and Genomes (KEGG) analysis. The Python SciPy package (version: 3.7.0; scipy.org/install/) was used for KEGG pathway enrichment analysis. To control the false positive rate, the Benjamini-Hochberg (HR) method was implemented for multiple testing correction. A corrected P-value threshold of 0.05 was established, with KEGG pathways meeting this criterion classified as significantly enriched.

Gene set enrichment analysis (GSEA). The GSEA analysis was conducted using the Majorbio Cloud Platform with standardized protocols (40). The platform's built-in preprocessing ensured proper gene ID conversion and low expression filtering prior to analysis. Gene expression data were analyzed against MSigDB Hallmark gene sets. Significant pathways were identified using the following thresholds: |NES|>1, FDR (q-value) <0.25, and P<0.05.

Encode data collection. Chromatin immunoprecipitation-sequencing data for H3K27ac in IMR90 (ENCFF694JJX) and A549 (ENCFF701DZR) cells were obtained from the ENCODE database (encodeproject.org/).

Statistical analysis. Data are presented as the mean ± standard deviation. All experiments were repeated at least twice. Data were analyzed using GraphPad Prism 9 (Dotmatics). One-way analysis of variance or unpaired two-tail student t-test was used to compare data. Tukey's Honestly Significant Difference test was performed as the post hoc analysis P<0.05 was considered to indicate a statistically significant difference.

Results

GPM6B serves as a prognostic marker and is expressed at low levels in LUAD. Survival outcomes associated with GPM6B in patients with LUAD were analyzed using the Kaplan-Meier plotter. Higher levels of GPM6B expression were associated with improved OS (Fig. 1A). A nomogram was developed to assess the impact of GPM6B on the prognosis of patients with LUAD (Fig. 1B). Clinical node and tumor stages are the primary predictors of survival, while age, sex, and GPM6B expression levels contributed smaller risks. In the GEPIA database and two GEO datasets (accession nos. GSE10072 and GSE115002), expression of GPM6B was revealed to be decreased in LUAD tissues when compared with normal tissues (Fig. 1C and D). In addition, GPM6B expression levels were negatively associated with cancer stages and nodal metastasis status (Fig. 1E and F). IHC staining of GPM6B revealed decreased expression of GPM6B in LUAD tissues compared with adjacent normal tissue (Fig. 1G).

GPM6B overexpression inhibits the proliferation, migration and invasion of LUAD cells. To elucidate the role of GPM6B in tumor pathogenesis, stable A549 and PC9 cell line with GPM6B overexpression were generated, as confirmed by RT-qPCR and western blot analysis (Fig. 2A and B). CCK-8 assay revealed that GPM6B overexpression significantly suppressed the proliferation of both LUAD cell lines at day 5 (Fig. 2C). Ki67 is a nuclear protein associated with cell cycle progression and proliferation (34). Flow cytometry revealed that Ki67 staining signal was lower in GPM6B-overexpressing LUAD compared with control cells (Fig. 2D). Additionally, Transwell assay demonstrated that GPM6B overexpression significantly suppressed migration and invasion of LUAD cells (Fig. 2E). Consistently, the wound healing assays confirmed the inhibitory role of GPM6B to cell migration in LUAD cells (Fig. 2F).

GPM6B overexpression upregulates the expression of HPGD. Transcriptome sequencing and data analysis were performed on GPM6B-overexpressing PC9 cells to identify the downstream genes and signaling pathways that are regulated by GPM6B. GPM6B affected the expression of 228 genes, including 120 upregulated and 108 downregulated genes (Fig. 3A). RT-qPCR was performed to identify the downstream genes, which revealed HPGD as a target gene (Fig. 3B). Furthermore, the protein levels of HPGD were increased in both LUAD cell lines overexpressing GPM6B (Fig. 3C). Survival analysis revealed that higher HPGD expression was associated with improved survival rates among patients with LUAD (Fig. 3D). Furthermore, the nomogram demonstrated an association between HPGD and clinical variables in predicting survival of patients with LUAD (Fig. 3E). Analysis of TCGA and GEO databases indicated that HPGD was downregulated in LUAD tissue (Fig. 3F and G). The expression of HPGD was lower in LUAD tissues than in normal tissue (Fig. 3H). Co-immunoprecipitation was used to further explore the relationship between GPM6B and HPGD, however, no interaction between GPM6B and HPGD was detected, suggesting that GPM6B regulated HPGD at the transcriptional level (Fig. 4A). Moreover, there was a positive association between HPGD and GPM6B expression levels (Fig. 4B and C). These findings collectively suggest that HPGD may be a target gene of GPM6B.

HPGD overexpression inhibits the proliferation, migration and invasion of the LUAD cel lines A549 and PC9. The

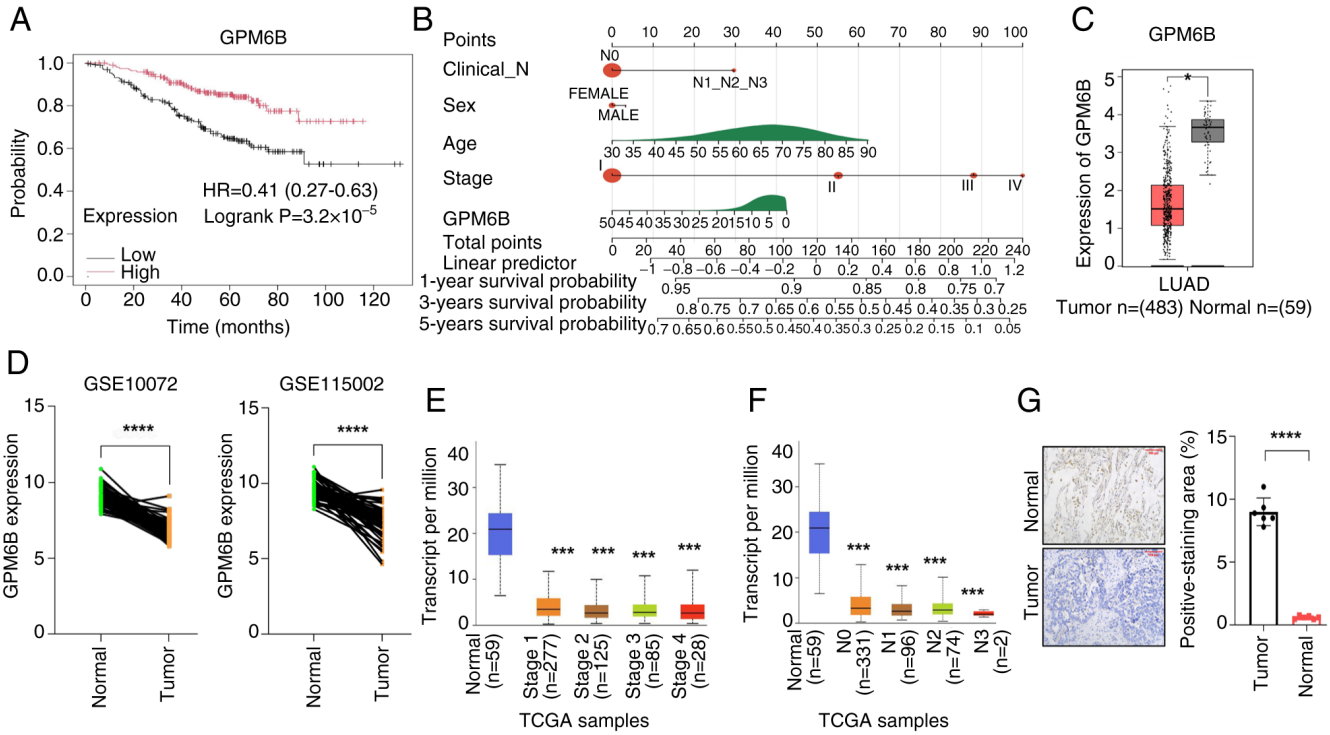

Figure 1. Association between GPM6B expression and prognosis of patients with LUAD. (A) Survival curve for the differential expression of GPM6B was analyzed using the Kaplan-Meier plotter. (B) Nomogram based on clinicopathological factors, including clinical N stage, sex, age, tumor stage and GPM6B expression. Differential expression of GPM6B in LUAD tumor and normal tissue based on the (C) Gene Expression Profiling Interactive Analysis and (D) Gene Expression Omnibus datasets. Differential expression of GPM6B based on (E) individual cancer stage and (F) nodal metastasis status. (G) IHC analysis of GPM6B in LUAD tissues and adjacent normal tissues. Scale bar, 100 μm. *P<0.05, ***P<0.001, ****P<0.0001 vs. normal. HR, hazard ratio; LUAD, lung adenocarcinoma; IHC, immunohistochemistry; GPM6B, Glycoprotein M6B; TCGA The Cancer Genome Atlas.

aforementioned results indicated GPM6B serves as a tumor suppressor and promotes HPGD expression in LUAD cells. Therefore, the effects of HPGD on cell proliferation and migration were investigated using gain-of-function studies in A549 and PC9 cells overexpressing HPGD. RT-qPCR and western blot analyses confirmed the increased expression of HPGD in both LUAD cell lines (Fig. 5A and B). Cells with increased HPGD levels exhibited decreased proliferation and migration capacities (Fig. 5C-F), similar to the effects observed in cells with elevated GPM6B expression levels. Overall, these findings suggested that GPM6B exerts its tumor-suppressive effects by transcriptionally regulating HPGD.

GPM6B overexpression activates the p53 signaling pathway. Gene Ontology analysis demonstrated that the differentially expressed genes were associated with 'regulation of apoptotic process', 'regulation of cell death', 'regulation of cell population proliferation', 'negative regulation of biological process' and 'tissue development' (Fig. 6A). Kyoto Encyclopedia of Genes and Genomes analysis indicated that GPM6B expression was associated with 'cellular senescence', 'cGMP-PKG signaling pathway', 'cytokine-cytokine receptor interaction', 'IL-17 signaling pathway', 'retinol metabolism' and 'p53 signaling pathway' (Fig. 6B). In addition, Gene Set Enrichment Analysis revealed that DNA replication, glycolysis, gluconeogenesis and glutathione metabolism were positively enriched in both GPM6B-overexpressing cell lines (Fig. 6C). Notably, GPM6B was associated with the p53 signaling pathway, which is frequently dysregulated in a number of human cancer types (41). Western blot analysis demonstrated that GPM6B overexpressing cells exhibited changes in expression of proteins involved in the p53 signaling pathway, including decreased expression of Bcl-2 and CCND1 and increased expression of p53 and Bax (Fig. 6D). This suggested that GPM6B may inhibit tumor development in LUAD by activating the p53 signaling pathway.

GPM6B overexpression suppresses tumor growth in vivo. Nude mouse xenografts with A549 cells overexpressing GPM6B were used to investigate the oncogenic role of GPM6B in LUAD progression (Fig. 7A). Tumor volume at day 33 and weight in the GPM6B-overexpressing mice were significantly lower compared with control mice (Fig. 7B-D). Compared with control mice, H&E staining in GPM6B-overexpressing mice revealed that dissected tissue cells had enlarged nuclei and the intercellular stroma was decreased, which were consistent with characteristics of tumor cells (Fig. 7E). Moreover, IHC analysis of the excised tumors revealed decreased Ki67 staining intensity in the GPM6B-overexpressing group (Fig. 7F). Taken together, these findings indicated that elevated GPM6B expression contributes to the decreased proliferative capacity of LUAD tumor cells.

DNA methylation and histone deacetylation inhibit GPM6B expression. As GPM6B expression was decreased in LUAD, the effect of DNA and H3K27 methylation and histone deacetylation on GPM6B levels was assessed. Disrupting expression of EZH2 did not alter expression of GPM6B,

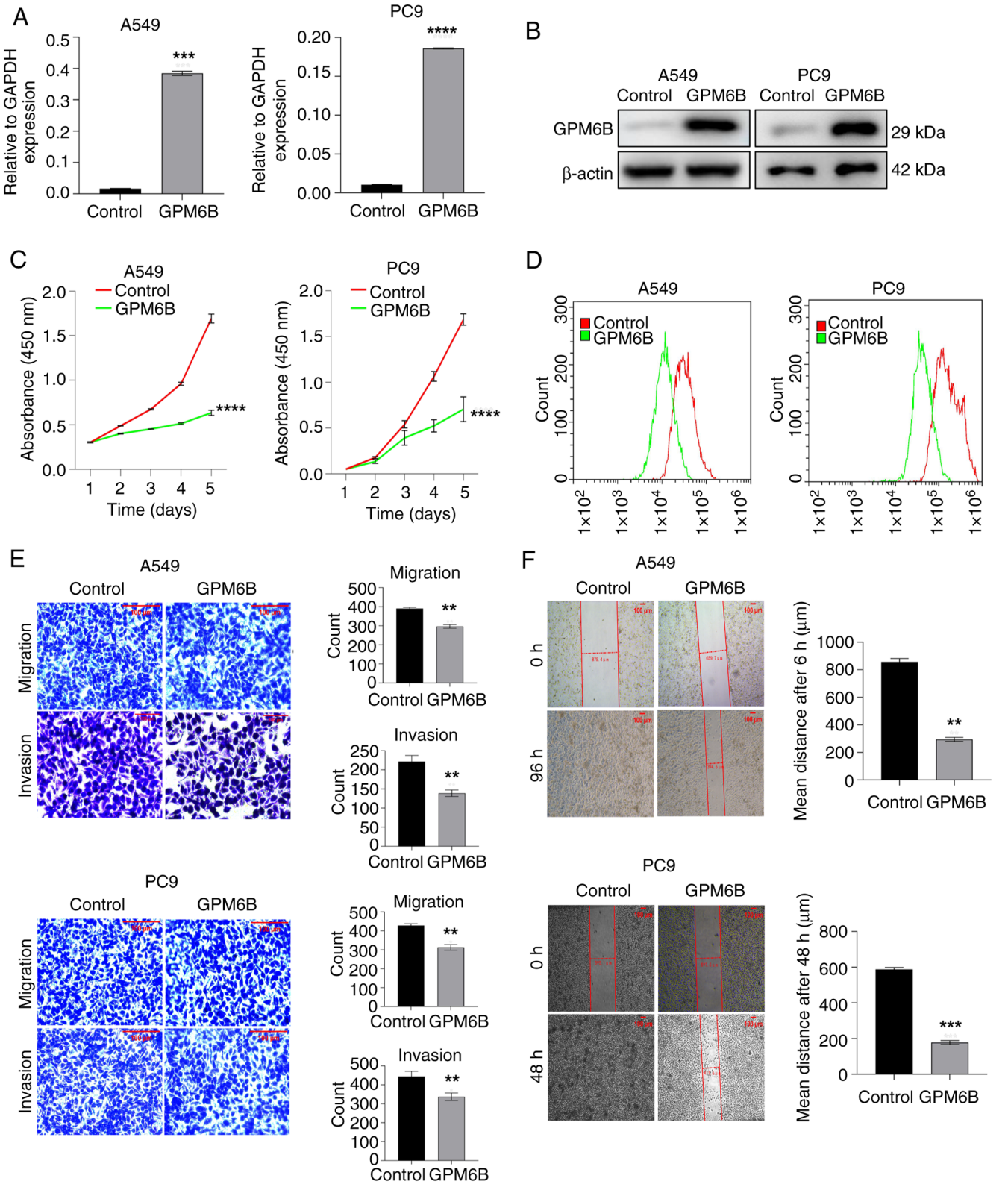

Figure 2. GPM6B regulates the proliferation, migration and invasion of LUAD cells. (A) Reverse transcription-quantitative PCR analysis and (B) western blot confirmation of GPM6B overexpression in LUAD cells A549 and PC9. (C) CCK-8 and (D) Ki67 staining assays depicting the decreased proliferation ability of GPM6B-overexpressing cells. (E) Transwell assays were used to determine the migration and invasion of GPM6B-overexpressing A549 and PC9 cells. (F) Wound healing assay was used to monitor the migration ability of GPM6B-overexpressing cells. **P<0.01, ***P<0.001, ****P<0.0001 vs. Control. (A,C) LUAD, lung adenocarcinoma; GPM6B, Glycoprotein M6B.

suggesting that EZH2-mediated H3K27 methylation was not responsible for the reduction in GPM6B expression levels (Fig. 8A). DNA methylation was subsequently evaluated at the GPM6B promoter region by exploring the UALCAN database. DNA methylation was significantly greater in LUAD compared with normal tissues (Fig. 8B). Histone acetylation at

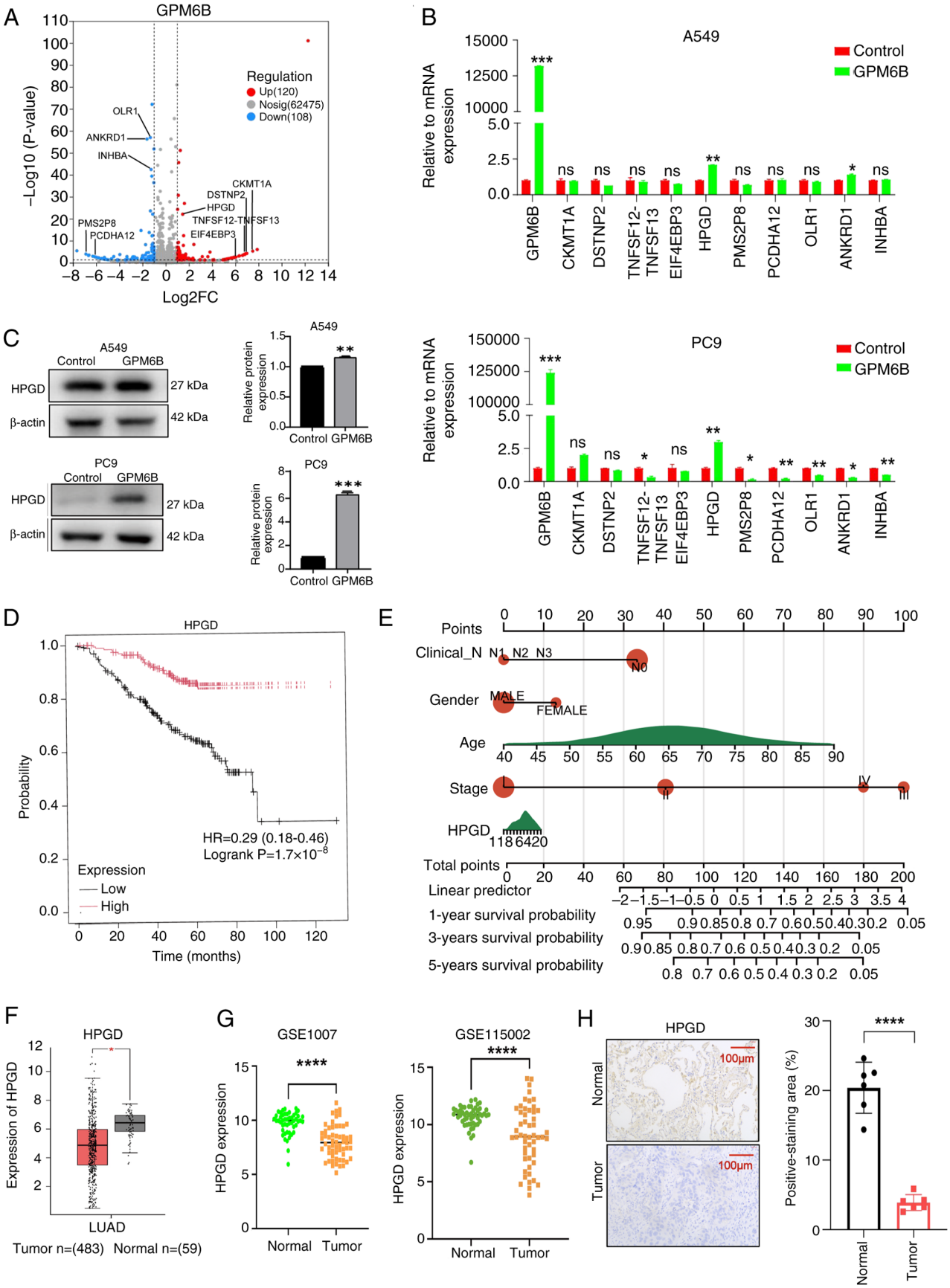

Figure 3. GPM6B regulates HPGD expression. (A) DEGs identified via transcriptome sequencing following GPM6B overexpression. (B) Reverse transcription-quantitative PCR validation of DEGs. (C) Western blot analysis of HPGD expression. (D) OS plot of HPGD in LUAD. (E) Nomogram was used to predict the OS probability of patients with LUAD at 1, 3 and 5 years. mRNA expression levels of HPGD in LUAD and paired adjacent normal tissue in (F) The Cancer Genome Atlas and (G) GSE10072 and GSE115002 datasets. (H) IHC analysis of HPGD in LUAD and adjacent normal tissues. Scale bar, 100 μm. *P<0.05 vs. Normal; **P<0.01, ***P<0.01, ****P<0.0001 vs. Control. (G, H) HPGD, 15-hydroxy prostaglandin dehydrogenase; DEG, differentially expressed gene; OS, overall survival; LUAD, lung adenocarcinoma; IHC, immunohistochemistry; ns, not significant.

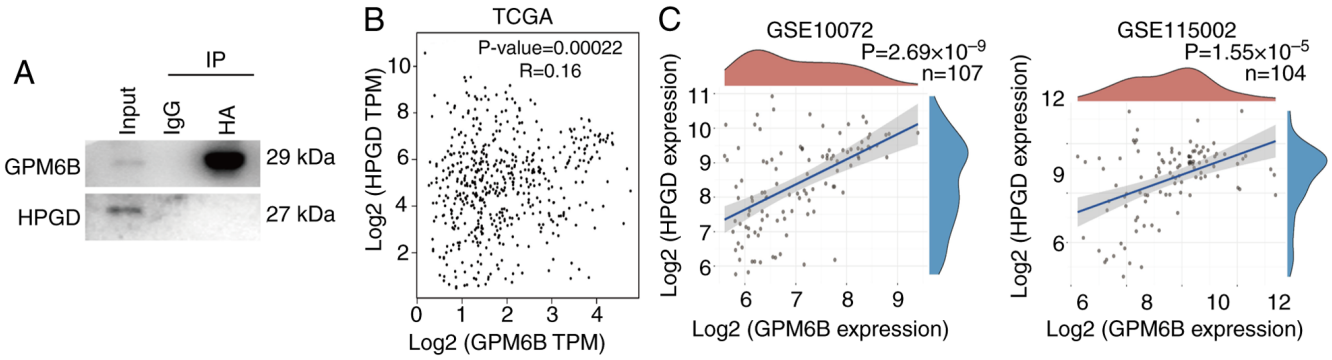

Figure 4. Association between GPM6B and HPGD. (A) Western blot showing the expression of GPM6B and HPGD in 293T cells transfected with HA-tagged GPM6B plasmid. Association between GPM6B and HPGD expression in (B) TCGA and (C) GSE10072 and GSE115002 datasets. HPGD, 15-hydroxy prostaglandin dehydrogenase; TGCA, The Cancer Genome Atlas; GPM6B, Glycoprotein M6B; IP, Immunoprecipitation; TPM, Transcripts Per Million.

the H3K27ac site, which can be inhibited by HDAC proteins, promotes chromatin relaxation and gene expression (42,43). Chromatin immunoprecipitation-seq data of H3K27ac in normal human embryonic lung fibroblasts (IMR90 cells) and LUAD (A549 cells) were downloaded from the ENCODE database. Enrichment of H3K27ac at the GPM6B promoter region was decreased in A549 cells compared with IMR90 cells (Fig. 8C). To investigate the effects of DNA methylation and histone deacetylation on GPM6B expression, their specific inhibitors DCA and TSA were used to treat LUAD cells. Based on the CCK-8 assay results, 100, 500 and 1,000 μM DCA was selected for treatment for 48 h and 1, 3 and 5 μM TSA was selected for treatment for 24 h in both LUAD cell lines (Fig. 8D and E). RT-qPCR results revealed that the expression level of GPM6B increased in a dose-dependent manner in response to treatment with DCA or TSA (Fig. 8F and G). These observations indicated that both DNA methylation and histone deacetylation are associated with the downregulation of the tumor suppressor gene GPM6B in LUAD cells.

Discussion

LUAD, the predominant subtype of lung cancer, originates from small airway epithelial and type II alveolar cells, and is one of the most lethal types of human cancer, which accounted for 18.7% of cancer-related deaths according to the global cancer statistics in 2022 (44,45). While patients with LUAD may benefit from targeted therapies, the OS of these patients remains <5 years, primarily due to the development of drug resistance and the occurrence of distant metastases (3,46). The aggressiveness of LUAD is promoted by the activation of oncogenes or inactivation of tumor suppressor genes (47). Identifying these dysregulated genes is key for enhancing diagnosis and treatment strategies for patients with LUAD.

The PLP family members serve a key role in myelination and neuroprotection, which are essential for cell differentiation and survival (48-51). GPM6B is a member of the PLP family and is abundant in the perinatal central nervous system (52). GPM6B is a potential oncogene associated with human lymphoid leukemia, yet paradoxically serves as a suppressor of tumor progression in prostate cancer, highlighting the multifaceted role of GPM6B in human cancer (29,53). Therefore, a deeper exploration is warranted to elucidate the function and underlying mechanisms of GPM6B in different types of cancer.

In the present study, GPM6B was identified as a tumor suppressor gene as it inhibited cell proliferation, migration and invasion in LUAD cells. While the Transwell experiment offers a rapid assessment of migration and invasion *in vitro*, the two-dimensional environment may not fully replicate the complex behaviors of cells *in vivo*. To address this limitation, future studies should perform 3D cell sphere migration and invasion assays, which provide a three-dimensional structure that more closely resembles the physiological environment. Investigating the expression of GPM6B in LUAD clinical samples may establish an association between GPM6B expression and clinical features.

Using transcriptome sequencing, HPGD was identified as a downstream effector of GPM6B. HPGD is a tumor suppressor that can inhibit cell proliferation and metastasis in various malignancies, such as gastrointestinal, bladder, lung and liver cancer (54-57). Moreover, the role of HPGD in maintaining tumor stemness has been recently uncovered (58). GPM6B is reported to influence tumor cell stemness by either enhancing aldehyde dehydrogenase 1 family member A1 expression or repressing the Wnt signaling pathway (30,59). Therefore, GPM6B may exert tumor suppressive effects by modulating the expression of HPGD. The p53 signaling pathway is one of the most frequently dysregulated pathways in tumor cells, serving a key role in the regulation of cell proliferation and apoptosis (41,60). The present study revealed that the overexpression of GPM6B led to an increase in expression of p53 and Bax, while simultaneously decreasing the levels of Bcl-2 and CCND1. This suggested that GPM6B may inhibit malignant behavior of LUAD cells by activating p53 signaling.

From an epigenetic perspective, decreased expression of GPM6B in LUAD cells may be caused by changes in DNA methylation and histone deacetylation. Hypermethylation of the promoter domain and condensation of the chromatin region provide docking sites for epigenetic regulatory factors and transcriptional suppressors to inhibit gene expression (61,62). The inhibitor of DNA methylation (DCA) used in the present study simultaneously targets DNMT1, DNMT3A and DNMT3B, whereas the inhibitor of histone deacetylation (TSA) concurrently targets class I and II HDACs (63-65). The combination of DNA-demethylation reagents and HDAC inhibitors exerts

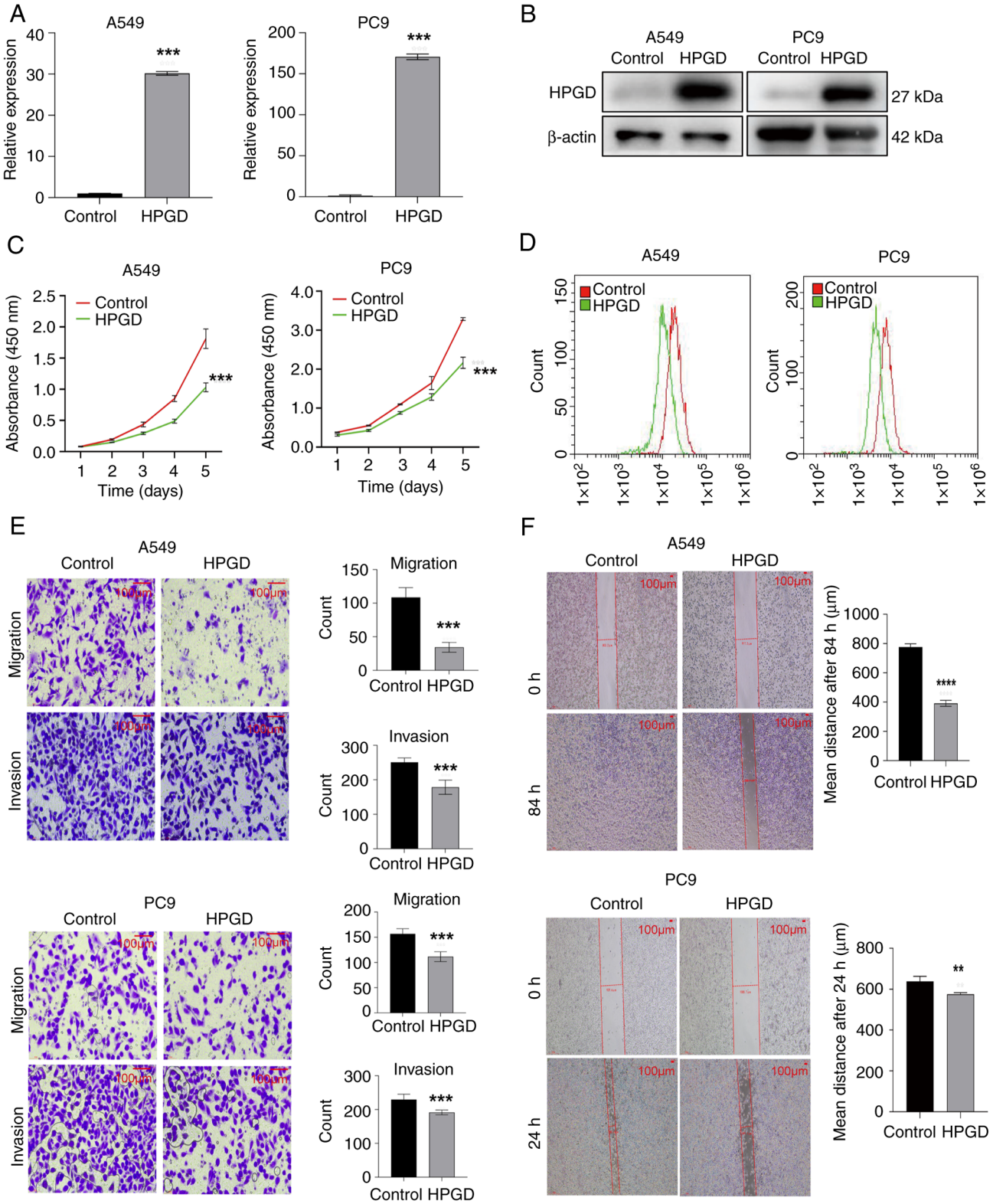

Figure 5. HPGD overexpression inhibits the proliferation, migration and invasion of LUAD cells. (A) Reverse transcription-quantitative PCR and (B) western blot confirmation of HPGD overexpression efficiency in LUAD cells. (C) Cell Counting Kit-8 and (D) Ki67 staining demonstrated reduced proliferation of HPGD-overexpressing cells. (E) Transwell assays were used to determine the migration and invasion of control and HPGD-overexpressing LUAD cells. (F) Wound healing assay was used to monitor the migration. **P<0.01, ***P<0.001, ****P<0.0001 vs. control. HPGD, 15-hydroxy prostaglandin dehydrogenase; LUAD, lung adenocarcinoma.

synergistic benefits in cancer treatment (66). Identifying the specific DNMTs and HDACs responsible for the suppression of GPM6B expression may improve understanding of the molecular mechanisms governing GPM6B expression in LUAD. Numerous HDAC inhibitors, including vorinostat, belinostat and Panobinostat (LBH-589), have been approved by the United States Food and Drug Administration for cancer treatment, and the treatment outcomes are promising when these agents are combined

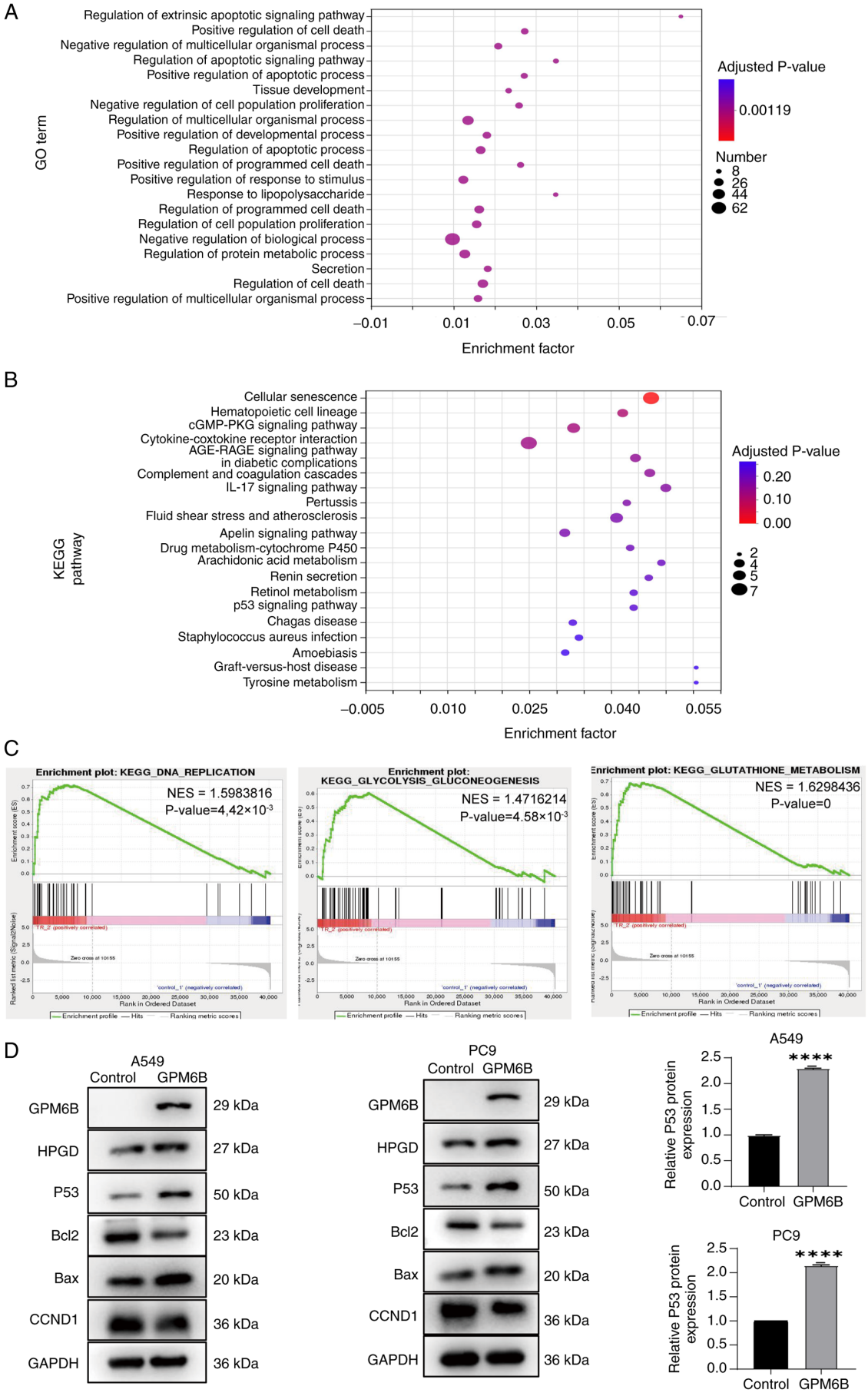

Figure 6. GPM6B overexpression activates p53 signaling pathway. (A) GO, (B) KEGG and (C) Gene Set Enrichment Analysis. (D) Western blot images revealed changes in the expression of GPM6B, HPGD, P53, CCND1, Bcl2 and Bax. ****P<0.0001 vs. Control. (D) GO, Gene Ontology; KEGG, Kyoto Encyclopedia of Genes and Genomes; GPM6B, Glycoprotein M6B; HPGD, 15-hydroxy prostaglandin dehydrogenase; CCND1, cyclin D1; NES, normalized enrichment score.

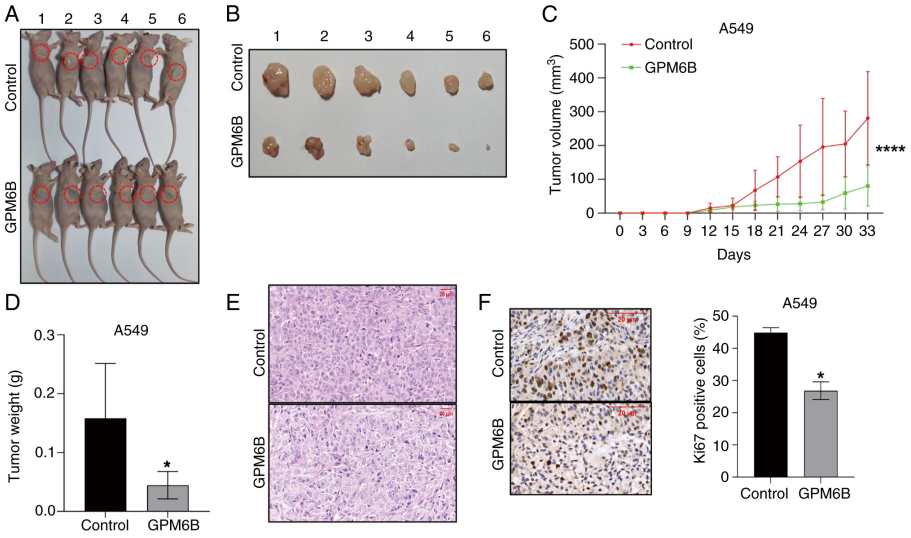

Figure 7. Overexpression of GPM6B suppresses LUAD tumor growth *in vivo*. (A) Subcutaneous tumors (circled in red for visualization. (B) Xenograft tumors in each group. (C) Changes in tumor volume. (D) Statistical histogram displaying the weights of xenograft tumors. (E) Representative hematoxylin and eosin staining. Scale bar, 20 μm. (F) Representative immunohistochemistry analysis of Ki67. Scale bar, 100 μm. *P<0.05, ****P<0.0001 vs. Control. LUAD, lung adenocarcinoma; GPM6B, Glycoprotein M6B.

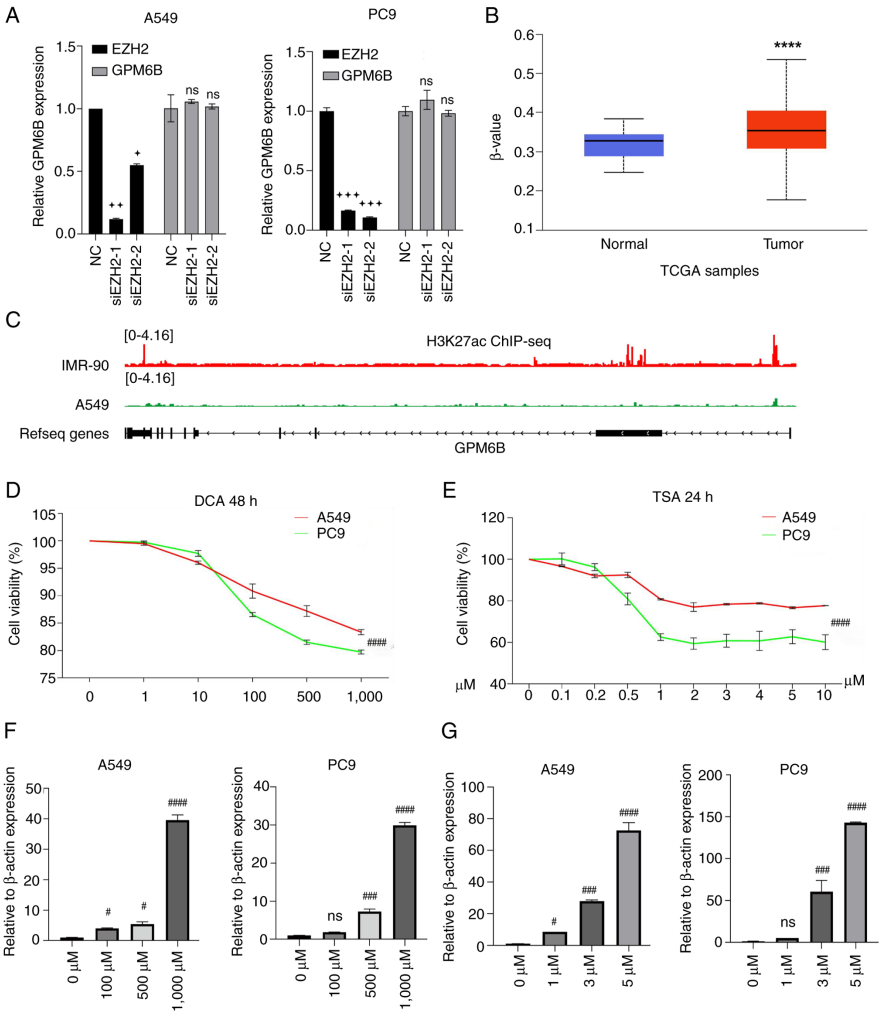

Figure 8. DNA methylation and histone deacetylation inhibit expression of GPM6B. (A) Reverse transcription-quantitative PCR analysis of GPM6B expression. (B) DNA methylation at the GPM6B promoter region. (C) Enrichment of H3K27ac at the GPM6B promoter region in IMR90 and A549 cells. The effects of (D) DCA and (E) TSA were measured using Cell Counting Kit-8 assay. The mRNA levels of GPM6B in control and (F) DCA or (G) TSA-treated LUAD cells. $^{+}$P<0.05, $^{++}$P<0.01, $^{+++}$P<0.001 vs. NC, ****P<0.0001 vs. Normal, $^{\#}$P<0.05, $^{\#\#\#}$P<0.001, $^{\#\#\#\#}$P<0.0001 vs. 0 μM. ns, not significant; EZH2, enhancer of zeste homolog 2; LUAD, lung adenocarcinoma; TCGA, The Cancer Genome Atlas; DCA, decitabine; TSA, trichostatin A; GPM6B, Glycoprotein M6B; NC, negative control; si, small interfering.

with primary chemotherapeutic agents (67,68). Consequently, the effects of GPM6B on chemotherapy sensitivity warrant exploring.

The present study revealed that DNA methylation and histone deacetylation were responsible for the diminished expression of GPM6B in LUAD cells. Overexpression of GPM6B suppressed cell proliferation and migration by increasing HPGD expression. In summary, the present study identified GPM6B as a novel therapeutic target for LUAD. Further exploration of molecular drugs targeting GPM6B may facilitate development of novel treatment strategies and improve patient survival.

Acknowledgements

Not applicable.

Funding

The present study was supported by the National Natural Science Foundation of China (grant no. 82103299), Natural Science Project of Anhui Province's Universities (grant no. 2022AH050790) and Fuyang City's '14th Five-Year Plan' Key Clinical Specialty Construction Project.

Availability of data and materials

The data generated in the present study may be found in the Gene Expression Omnibus (GEO) dataset under the accession number GSE261836 or at the following URL: https://www.ncbi.nlm.nih.gov/geo/query/acc.cgi?acc=GSE261836.

Authors' contributions

YL and XY performed experiments, constructed the figures and wrote the manuscript. QC, YM, XF and GL performed experiments. HZ analyzed data. QD and LZ designed the project and revised the manuscript. YL, QD and LZ confirm the authenticity of all the raw data. All authors have reviewed and approved the final manuscript.

Ethics approval and consent to participate

All experiments were reviewed and approved by the Ethics Committee of Anhui Medical University (approval nos. KYXM-202410-010 and LLSC20242301). All procedures were conducted in accordance with relevant guidelines and regulations, adhering to the ARRIVE guidelines.

Patient consent for publication

Not applicable.

Competing interests

The authors declare that they have no competing interests.

References

1. Kratzer TB, Bandi P, Freedman ND, Smith RA, Travis WD, Jemal A and Siegel RL: Lung cancer statistics, 2023. Cancer 130: 1330-1348, 2024.
2. Siegel RL, Kratzer TB, Giaquinto AN, Sung H and Jemal A: Cancer statistics, 2025. CA Cancer J Clin 75: 10-45, 2025.
3. Denisenko TV, Budkevich IN and Zhivotovsky B: Cell death-based treatment of lung adenocarcinoma. Cell Death Dis 9: 117, 2018.
4. Wu SG and Shih JY: Management of acquired resistance to EGFR TKI-targeted therapy in advanced non-small cell lung cancer. Mol Cancer 17: 38, 2018.
5. Lim SM, Syn NL, Cho BC and Soo RA: Acquired resistance to EGFR targeted therapy in non-small cell lung cancer: Mechanisms and therapeutic strategies. Cancer Treat Rev 65: 1-10, 2018.
6. Imyanitov EN, Iyevleva AG and Levchenko EV: Molecular testing and targeted therapy for Non-small cell lung cancer: Current status and perspectives. Crit Rev Oncol Hematol 157: 103194, 2021.
7. Lamberti G, Andrini E, Sisi M, Rizzo A, Parisi C, Di Federico A, Gelsomino F and Ardizzoni A: Beyond EGFR, ALK and ROS1: Current evidence and future perspectives on newly targetable oncogenic drivers in lung adenocarcinoma. Crit Rev Oncol Hematol 156: 103119, 2020.
8. Xia L, Liu Y and Wang Y: PD-1/PD-L1 blockade therapy in advanced Non-Small-cell lung cancer: Current status and future directions. Oncologist 24 (Suppl 1): S31-S41, 2019.
9. Mamdani H, Matosevic S, Khalid AB, Durm G and Jalal SI: Immunotherapy in lung cancer: Current landscape and future directions. Front Immunol 13: 823618, 2022.
10. Wang S, Wang Y, Wu X, Yang L and Zhang X: Patients outcomes in lung adenocarcinoma transforming to small-cell lung cancer after tyrosine kinase inhibitor therapy. World J Surg Oncol 23: 34, 2025.
11. Zha J, Li J, Yin H, Shen M and Xia Y: TIMM23 overexpression drives NSCLC cell growth and survival by enhancing mitochondrial function. Cell Death Dis 16: 174, 2025.
12. Leonetti A, Sharma S, Minari R, Perego P, Giovannetti E and Tiseo M: Resistance mechanisms to osimertinib in EGFR-mutated non-small cell lung cancer. Br J Cancer 121: 725-737, 2019.
13. Chao YL and Pecot CV: Targeting epigenetics in lung cancer. Cold Spring Harb Perspect Med 11: a038000, 2021.
14. Dong N, Shi L, Wang DC, Chen C and Wang X: Role of epigenetics in lung cancer heterogeneity and clinical implication. Semin Cell Dev Biol 64: 18-25, 2017.
15. Liu Y, Hu X, Han C, Wang L, Zhang X, He X and Lu X: Targeting tumor suppressor genes for cancer therapy. Bioessays 37: 1277-1286, 2015.
16. Moore LD, Le T and Fan G: DNA methylation and its basic function. Neuropsychopharmacology 38: 23-38, 2013.
17. Bajbouj K, Al-Ali A, Ramakrishnan RK, Saber-Ayad M and Hamid Q: Histone modification in NSCLC: Molecular mechanisms and therapeutic targets. Int J Mol Sci 22: 11701, 2021.
18. Laugesen A, Hojfeldt JW and Helin K: Molecular mechanisms directing PRC2 recruitment and H3K27 methylation. Mol Cell 74: 8-18, 2019.
19. Belinsky SA: Gene-promoter hypermethylation as a biomarker in lung cancer. Nat Rev Cancer 4: 707-717, 2004.
20. Yang X, Shi W, Huang X, Hu L, Wang J, Zhang F, Wang Y and Huang K: Low-level EFCAB1 promoted progress by upregulated DNMT3B and could be as a potential biomarker in lung adenocarcinoma. J Clin Lab Anal 36: e24166, 2022.
21. Tan M, Wu J and Cai Y: Suppression of Wnt signaling by the miR-29 family is mediated by demethylation of WIF-1 in non-small-cell lung cancer. Biochem Biophys Res Commun 438: 673-679, 2013.
22. Duan R, Du W and Guo W: EZH2: A novel target for cancer treatment. J Hematol Oncol 13: 104, 2020.
23. Gao M, Li Y, Cao P, Liu H, Chen J and Kang S: Exploring the therapeutic potential of targeting polycomb repressive complex 2 in lung cancer. Front Oncol 13: 1216289, 2023.
24. Shin DS, Park K, Garon E and Dubinett S: Targeting EZH2 to overcome the resistance to immunotherapy in lung cancer. Semin Oncol 49: 306-318, 2022.
25. Werner H, Dimou L, Klugmann M, Pfeiffer S and Nave KA: Multiple splice isoforms of proteolipid M6B in neurons and oligodendrocytes. Mol Cell Neurosci 18: 593-605, 2001.
26. Werner HB, Kramer-Albers EM, Strenzke N, Saher G, Tenzer S, Ohno-Iwashita Y, De Monasterio-Schrader P, Möbius W, Moser T, Griffiths IR and Nave KA: A critical role for the cholesterol-associated proteolipids PLP and M6B in myelination of the central nervous system. Glia 61: 567-586, 2013.
27. Honda A, Ito Y, Takahashi-Niki K, Matsushita N, Nozumi M, Tabata H, Takeuchi K and Igarashi M: Extracellular signals induce glycoprotein M6a clustering of lipid rafts and associated signaling molecules. J Neurosci 37: 4046-4064, 2017.

28. Zhu Y, Wang Q, Xia Y, Xiong X, Weng S, Ni H, Ye Y, Chen L, Lin J, Chen Y, *et al*: Evaluation of MiR-1908-3p as a novel serum biomarker for breast cancer and analysis its oncogenic function and target genes. BMC Cancer 20: 644, 2020.
29. He S, Huang Z, Li X, Ding Y, Sheng H, Liu B and Jia Z: GPM6B inhibit PCa proliferation by blocking prostate cancer cell serotonin absorptive capacity. Dis Markers 2020: 8810756, 2020.
30. Miao Z, Geng L, Xu L, Ye Y, Wu C, Tian W and Liu N: Integrated analysis reveals prognostic value and mesenchymal identity suppression by glycoprotein M6B in glioma. Am J Transl Res 14: 3052-3065, 2022.
31. Clough E and Barrett T: The gene expression omnibus database. Methods Mol Biol 1418: 93-110, 2016.
32. Tomczak K, Czerwinska P and Wiznerowicz M: The cancer genome atlas (TCGA): An immeasurable source of knowledge. Contemp Oncol (Pozn) 19: A68-A77, 2015.
33. Livak KJ and Schmittgen TD: Analysis of relative gene expression data using real-time quantitative PCR and the 2(-Delta Delta C(T)) method. Methods 25: 402-408, 2001.
34. Li LT, Jiang G, Chen Q and Zheng JN: Ki67 is a promising molecular target in the diagnosis of cancer (review). Mol Med Rep 11: 1566-1572, 2015.
35. Menon SS, Guruvayoorappan C, Sakthivel KM and Rasmi RR: Ki-67 protein as a tumour proliferation marker. Clin Chim Acta 491: 39-45, 2019.
36. Jurikova M, Danihel L, Polak S and Varga I: Ki67, PCNA, and MCM proteins: Markers of proliferation in the diagnosis of breast cancer. Acta Histochem 118: 544-552, 2016.
37. Han T, Zhan W, Gan M, Liu F, Yu B, Chin YE and Wang JB: Phosphorylation of glutaminase by PKCepsilon is essential for its enzymatic activity and critically contributes to tumorigenesis. Cell Res 28: 655-669, 2018.
38. Wu J, Zhao Q, Chen S, Xu H, Zhang R, Cai D, Gao Y, Peng W, Chen X, Yuan S, *et al*: NSUN4-mediated m5C modification of circERI3 promotes lung cancer development by altering mitochondrial energy metabolism. Cancer Lett 605: 217266, 2024.
39. Xu Y, Hu Y, Xu T, Yan K, Zhang T, Li Q, Chang F, Guo X, Peng J, Li M, *et al*: RNF8-mediated regulation of Akt promotes lung cancer cell survival and resistance to DNA damage. Cell Rep 37: 109854, 2021.
40. Ren Y, Yu G, Shi C, Liu L, Guo Q, Han C, Zhang D, Zhang L, Liu B, Gao H, *et al*: Majorbio cloud: A One-stop, comprehensive bioinformatic platform for multiomics analyses. Imeta 1: e12, 2022.
41. Liu Y, Su Z, Tavana O and Gu W: Understanding the complexity of p53 in a new era of tumor suppression. Cancer Cell 42: 946-967, 2024.
42. Zhu M, Han Y, Gu T, Wang R, Si X, Kong D, Zhao P, Wang X, Li J, Zhai X, *et al*: Class I HDAC inhibitors enhance antitumor efficacy and persistence of CAR-T cells by activation of the Wnt pathway. Cell Rep 43: 114065, 2024.
43. Ling H, Li Y, Peng C, Yang S and Seto E: HDAC10 inhibition represses melanoma cell growth and BRAF inhibitor resistance via upregulating SPARC expression. NAR Cancer 6: zcae018, 2024.
44. Bray F, Laversanne M, Sung H, Ferlay J, Siegel RL, Soerjomataram I and Jemal A: Global cancer statistics 2022: GLOBOCAN estimates of incidence and mortality worldwide for 36 cancers in 185 countries. CA Cancer J Clin 74: 229-263, 2024.
45. Hendriks LEL, Remon J, Faivre-Finn C, Garassino MC, Heymach JV, Kerr KM, Tan DSW, Veronesi G and Reck M: Non-small-cell lung cancer. Nat Rev Dis Primers 10: 71, 2024.
46. Copur MS, Crockett D, Gauchan D, Ramaekers R and Mleczko K: Molecular testing guideline for the selection of patients with lung cancer for targeted therapy. J Clin Oncol 36: 2006, 2018.
47. Zito Marino F, Bianco R, Accardo M, Ronchi A, Cozzolino I, Morgillo F, Rossi G and Franco R: Molecular heterogeneity in lung cancer: From mechanisms of origin to clinical implications. Int J Med Sci 16: 981-989, 2019.
48. Brown FR III, Beck JC, Niebyl JR and Singh I: Effect of proteolipid protein on central nervous system myelin membrane fluidity. Neurosci Lett 59: 149-154, 1985.
49. Mobius W, Patzig J, Nave KA and Werner HB: Phylogeny of proteolipid proteins: Divergence, constraints, and the evolution of novel functions in myelination and neuroprotection. Neuron Glia Biol 4: 111-127, 2008.
50. Sapirstein VS, Nolan C, Stern R, Ciocci M and Masur SK: Identification of the plasma membrane proteolipid protein as a constituent of brain coated vesicles and synaptic plasma membrane. J Neurochem 51: 925-933, 1988.
51. Fernandez ME, Alfonso J, Brocco MA and Frasch AC: Conserved cellular function and Stress-mediated regulation among members of the proteolipid protein family. J Neurosci Res 88: 1298-1308, 2010.
52. Vouyiouklis DA, Werner H, Griffiths IR, Stewart GJ, Armin-Nave K and Thomson CE: Molecular cloning and transfection studies of M6b-2, a novel splice variant of a member of the PLP-DM20/M6 gene family. J Neurosci Res 52: 633-640, 1998.
53. Charfi C, Edouard E and Rassart E: Identification of GPM6A and GPM6B as potential new human lymphoid leukemia-associated oncogenes. Cell Oncol (Dordr) 37: 179-191, 2014.
54. Yan M, Rerko RM, Platzer P, Dawson D, Willis J, Tong M, Lawrence E, Lutterbaugh J, Lu S, Willson JK, *et al*: 15-Hydroxyprostaglandin dehydrogenase, a COX-2 oncogene antagonist, is a TGF-beta-induced suppressor of human gastrointestinal cancers. Proc Natl Acad Sci USA 101: 17468-17473, 2004.
55. Gee JR, Montoya RG, Khaled HM, Sabichi AL and Grossman HB: Cytokeratin 20, AN43, PGDH, and COX-2 expression in transitional and squamous cell carcinoma of the bladder. Urol Oncol 21: 266-270, 2003.
56. Ding Y, Tong M, Liu S, Moscow JA and Tai HH: NAD+-linked 15-hydroxyprostaglandin dehydrogenase (15-PGDH) behaves as a tumor suppressor in lung cancer. Carcinogenesis 26: 65-72, 2005.
57. Sun L, Suo C, Zhang T, Shen S, Gu X, Qiu S, Zhang P, Wei H, Ma W, Yan R, *et al*: ENO1 promotes liver carcinogenesis through YAP1-dependent arachidonic acid metabolism. Nat Chem Biol 19: 1492-1503, 2023.
58. Shu L, Li X, Liu Z, Li K, Shi A, Tang Y, Zhao L, Huang L, Zhang Z, Zhang D, *et al*: Bile exosomal miR-182/183-5p increases cholangiocarcinoma stemness and progression by targeting HPGD and increasing PGE2 generation. Hepatology 79: 307-322, 2023.
59. Kusumoto S, Ikeda JI, Kurashige M, Maeno-Fujinami E, Tahara S, Matsui T, Nojima S, Okuzaki D and Morii E: Tumor cell plasticity in endometrioid carcinoma is regulated by neuronal membrane glycoprotein M6-b. Oncol Lett 25: 45, 2023.
60. Ruiz-Losada M, Gonzalez R, Peropadre A, Gil-Gálvez A, Tena JJ, Baonza A and Estella C: Coordination between cell proliferation and apoptosis after DNA damage in Drosophila. Cell Death Differ 29: 832-845, 2022.
61. Meng H, Cao Y, Qin J, Song X, Zhang Q, Shi Y and Cao L: DNA methylation, its mediators and genome integrity. Int J Biol Sci 11: 604-617, 2015.
62. Gallinari P, Di Marco S, Jones P, Pallaoro M and Steinkuhler C: HDACs, histone deacetylation and gene transcription: From molecular biology to cancer therapeutics. Cell Res 17: 195-211, 2007.
63. Yu J, Qin B, Moyer AM, Nowsheen S, Liu T, Qin S, Zhuang Y, Liu D, Lu SW, Kalari KR, *et al*: DNA methyltransferase expression in triple-negative breast cancer predicts sensitivity to decitabine. J Clin Invest 128: 2376-2388, 2018.
64. Wong KK, Lawrie CH and Green TM: Oncogenic roles and inhibitors of DNMT1, DNMT3A, and DNMT3B in acute myeloid leukaemia. Biomark Insights 14: 1177271919846454, 2019.
65. Chang J, Varghese DS, Gillam MC, Peyton M, Modi B, Schiltz RL, Girard L and Martinez ED: Differential response of cancer cells to HDAC inhibitors trichostatin A and depsipeptide. Br J Cancer 106: 116-125, 2012.
66. Zahnow CA, Topper M, Stone M, Murray-Stewart T, Li H, Baylin SB and Casero RA Jr: Inhibitors of DNA methylation, histone deacetylation, and histone demethylation: A perfect combination for cancer therapy. Adv Cancer Res 130: 55-111, 2016.
67. Soflaei SS, Momtazi-Borojeni AA, Majeed M, Derosa G, Maffioli P and Sahebkar A: Curcumin: A natural Pan-HDAC inhibitor in cancer. Curr Pharm Des 24: 123-129, 2018.
68. Li Y and Seto E: HDACs and HDAC inhibitors in cancer development and therapy. Cold Spring Harb Perspect Med 6: a026831, 2016.